
Effect of MnO₂ doping on the dielectric properties of barium titanate ceramics *

¹Sitko D., ¹Bąk W., ¹Garbarz-Głos B., ²Antonova M. and
¹Jankowska-Sumara I.

¹Institute of Physics, Pedagogical University, Podchorążych 2, 30-084 Kraków, Poland, e-mail: dsitko@up.krakow.pl

²Institute of Solid State Physics, University of Latvia, Kengeraga 8, LV-1063, Riga, Latvia

Received: 09.09.2012

Abstract. The effect of MnO₂ doping on the structure, microstructure and dielectric properties of BaTiO₃ has been studied. For this purpose MnO₂-doped BaTiO₃ ceramics have been prepared using a conventional ceramic method. The energy-dispersive X-ray spectroscopy investigations have revealed that the samples BaTiO₃ + *x* wt. % MnO₂ (*x* = 0.01; 0.1) are perfectly sintered. Our studies have shown that all the electric parameters under investigation depend on the frequency of electric field and the amount of manganese substitution. In order to understand better the character of phase transition in BaTiO₃ + *x* wt. % MnO₂ (*x* = 0.01; 0.1), we have also studied the thermal behaviour of these compounds.

Keywords: BaTiO₃ doped with Mn, DSC, dielectric spectroscopy

PACS: 77.80.B-, 77.80.bg

UDC: 536, 537

1. Introduction

Barium titanate BaTiO₃ abbreviated hereafter as BT has been the first piezoelectric ceramics ever discovered and, due to its excellent ferroelectric properties and high dielectric constant at the room temperature, it is still widely used in capacitors, thermistors, chemical sensors and piezoelectric devices [1, 2]. Due to a great technological interest, titanate perovskites are also a focus of numerous applications.

The crystal structures typical for polycrystalline BaTiO₃ ceramics are denoted as h-BT (hexagonal), c-BT (cubic), t-BT (tetragonal), o-BT (orthorhombic), and r-BT (rhombohedral). The temperatures for the hexagonal–cubic (T_{h-c}), cubic–tetragonal (T_{c-t}), tetragonal–orthorhombic (T_{t-o}) and orthorhombic–rhombohedral (T_{o-r}) phase transitions are about 1703, 401, 285 and 202 K, respectively [3–6]. The structure of BaTiO₃ may be described as a combination of corner TiO₆ octahedra, with Ti⁴⁺ ions occupying a centre and Ba²⁺ ions located in the spaces among these octahedra. Because of some distortion, the octahedra are coupled together, thus causing a spontaneous polarisation and giving rise to a large dielectric constant and its significant temperature dependence.

There are many ways to dope BT, including transition metals [11, 12] or some others atoms [13, 14], and even organic materials [15]. Different admixtures have been introduced into bulk to substitute Ba²⁺ or Ti⁴⁺ [10]. When an impurity is introduced, the properties of the compound can

* The materials of this work have been reported at the 2nd Ukrainian–Polish–Lithuanian Meeting on Ferroelectrics Physics (9–13 September 2012, Lviv, Ukraine).

change dramatically. In particular, a lattice deformation occurs when the BT is doped with the transition metals. Kirianov et al. [7] have reported that doping with Mn would promote the transition from the tetragonal to cubic phases. At the same time, the authors of the works [5, 7] have argued that transformation from the tetragonal to hexagonal phases is observed. Therefore the role of Mn has not yet been completely understood. Notice that the manganese-modified BT ceramics have also been reported as a potential candidate for using in dielectric resonators [1].

The purpose of this work is to understand better the effect of Mn doping upon ferroelectric properties of BaTiO₃. For this aim we perform precise measurements of chemical composition, as well as thermal and dielectric properties.

2. Experimental procedures

Polycrystalline samples of BaTiO₃ + x wt. % MnO₂ ($x = 0.01; 0.1$) were prepared using a solid-state synthesis. The samples were synthesised from an analytically pure barium carbonate BaCO₃, titanium oxide TiO₂, and manganese oxide MnO₂. A mixture of the raw materials was homogenised and ground in an agate ball mill in ethanol for 24 h. The dried material was calcined at the temperature of 1523 K for 1–2 h. After the calcination, the powder was ground in ethanol, then cold-pressed (100 MPa) and sintered for 2 h with the aid of a conventional ceramic technology in the temperature region 1633–1693 K, depending on the composition.

The microstructure of the surface of our polycrystalline samples was examined using a SEM Model Hitachi S4700 with a field emission and a Noran Vantage EDS system.

An X-ray EDS (Energy-Dispersive X-ray Spectroscopy) microanalysis was applied to investigate the homogeneity of composition and an EPMA (Electron Probe Microbeam Analysis) was used to analyse the distribution of elements at the sample surface. Investigations of the chemical composition were performed using a Noran-Vantage microanalyser, which was a part of a Hitachi SEM. The use of a lithium-drifted siliceous detector with a multi-channel pulse height analyser enabled us to obtain diffraction patterns in any chosen micro-regions of sample surfaces.

Standard differential scanning calorimetry (DSC) measurements were performed with the aid of a Netzsch DSC F3 Maia apparatus equipped with an intra-cooler unit. A DSC scan provided an easy way to identify the phase transition temperatures for the ferroelectric ceramics. In particular, the endothermic peaks observed by us corresponded to the phase transitions. The samples were measured in the temperature region 150–600 K, using heating or cooling rates (10 K/min) in an argon atmosphere (30 cm³/min). The masses of our samples were about 50 mg. Because the temperature history of samples might affect the result, the DSC measurements were undertaken two times, one by one, and the second curve was treated as a final outcome.

The electric measurements of our samples were performed using an LCR Agilent 4284A meter and a temperature controlling system Quatro Krio 4.0. Temperature and frequency dependences of the dielectric permittivity, dielectric loss tangent and the electric conductivity were investigated in the temperature region 150–500 K at the frequencies of 20 Hz, 100 Hz, 1 kHz, 100 kHz and 1 MHz.

3. Results and discussion

3.1 Morphological and chemical investigations

The SEM investigations of the microstructure of our ceramics were performed on the fractures prepared in a way described above. The surface SEM investigations were performed on both Mn-doped and undoped BT samples. The SEM image of BaTiO₃ shows that its microstructure consists of inter-granular pores and grains of various sizes (the average grain size is estimated to be about

10 μm), with well-defined grain boundaries. A glassy phase is hard to find. The growth terraces are seen, which indicates that the growth of grains occurs according to a layer mechanism.

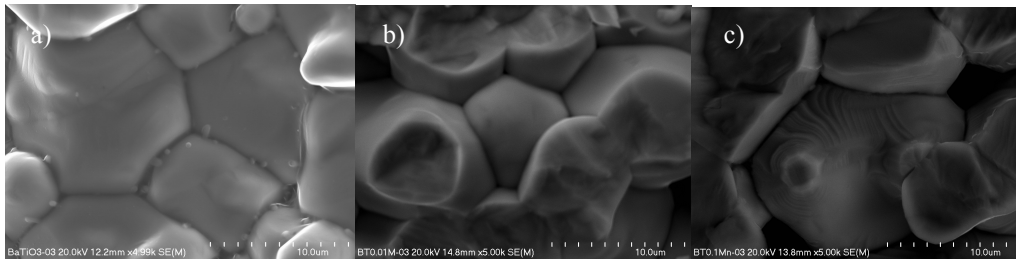


Fig. 1. SEM images of ceramics BaTiO_3 (a), $\text{BaTiO}_3 + 0.01 \text{ wt. \% MnO}_2$ (b) and $\text{BaTiO}_3 + 0.1 \text{ wt. \% MnO}_2$ (c) (magnification 5000 \times).

The SEM images of the samples with $x = 0.01$ and $x = 0.1$ (see Fig. 1b and 1c) indicate that the MnO_2 admixture does not influence drastically the microstructure. All the samples reveal almost equal densities, with comparable grain sizes. Only for the case of $x = 0.1$ one can observe that MnO_2 used as an admixture has an inhibiting effect on the grain growth process and, consequently, a relatively homogeneous microstructure arises, with higher amounts of inter-granular porosity and the grains $\sim 20\%$ larger than those typical for the non-modified sample. This may be due to the behavior of Mn - ions in the BaTiO_3 ceramics.

The EDS investigations (see Fig. 2) show that the ceramics $\text{BaTiO}_3 + x \text{ wt. \% MnO}_2$ ($x = 0.01; 0.1$) contain Ba, Ti, O and Mn elements near their surfaces. No other impurity element has been detected in the spectrum. The homogeneity of element distribution in the samples has been investigated with the EPMA method using an X-ray microprobe.

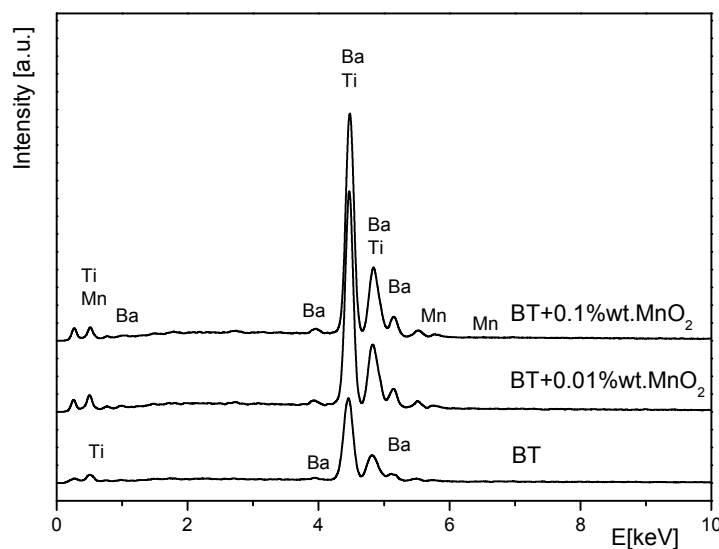


Fig. 2. EDS-peaks for BaTiO_3 , $\text{BaTiO}_3 + 0.01 \text{ wt. \% MnO}_2$ and $\text{BaTiO}_3 + 0.1 \text{ wt. \% MnO}_2$ ceramics.

The ‘mappings’ obtained by us have confirmed a qualitative composition presumed for the samples under examination. For all of the samples, the stoichiometric compositions have been examined, too. We have received the Ba/Ti ratios equal to 0.973 for the undoped BaTiO_3 , and 0.931 and 0.928 for $\text{BaTiO}_3 + x \text{ wt. \% MnO}_2$ ($x = 0.01$ and 0.1), respectively.

3.2 Thermodynamic investigations

In order to understand how thermodynamic properties are related to manganese content in the substituted BaTiO₃, the thermodynamic quantities such as the phase transition temperature and the enthalpy in the perovskite phase have been investigated in a wide temperature range (150–700 K), using a standard DSC technique. All the results normalised to the sample masses are plotted in Fig. 3. As seen from Fig. 3, the DSC data exhibit three distinct exothermic peaks for the BT, BaTiO₃ + 0.01 wt. % MnO₂ and BaTiO₃ + 0.1 wt. % MnO₂ samples.

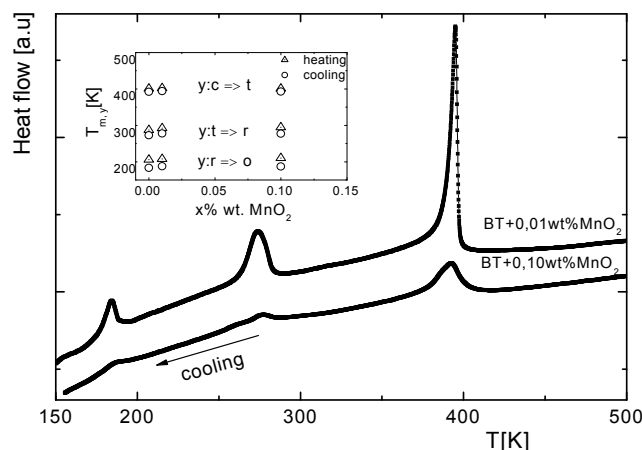


Fig. 3. Differential scanning calorimetric data for the ceramics BaTiO₃ + 0.01 wt. % MnO₂ and BaTiO₃ + 0.1 wt. % MnO₂. Insert shows phase transition temperatures observed on heating and cooling (DSC scan rate is 10 K/min).

In the case of pure BaTiO₃, the temperatures of the cubic–tetragonal phase transition are 403 K and 391 K, those between the tetragonal and orthorhombic structures are 287 and 273 K, and those between the orthorhombic and rhombohedral ones are 206 and 184 K on heating and cooling, respectively. All the data are collected in Fig. 3 (see the insert).

A special attention was paid to the samples with the Mn-ion admixture. For the system BaTiO₃ + 0.01 wt. % MnO₂, the first sharp peaks corresponding to the transition temperatures from the cubic to tetragonal phases are observed at 403 K and 393 K on heating and cooling, respectively. The second peaks are due to structural transformation from the tetragonal to orthorhombic phases. They are observed at 293 K and 295 K on heating and cooling, respectively. Finally, the third peaks correspond to orthorhombic–rhombohedral transformation. These peaks occur at about 208 K and 188 K in the heating and cooling runs, respectively. In addition, our analysis of the shape of these peaks and the energy exchange suggest that the phase transition is of the first order. All the transition temperatures mentioned above are almost equal for the sample doped with Mn ions and those of the pure BT.

The DSC run obtained for BaTiO₃ + 0.1 wt. % MnO₂ is totally different. As seen from Fig.3, only one broad peak and two humps are observed. Basing on the data obtained for the thermodynamic properties of BaTiO₃, one can assume that the peculiarity observed at 401 K in the cooling process (the temperature being very close to that observed for the pure BT) is associated with the structural transition between the cubic and tetragonal phases. The peak magnitude is only one-fourth of that corresponding to transformation from the cubic to tetragonal phases in BaTiO₃ + 0.01 wt. % MnO₂ sample. A lack of intensity in the phase transition peak can be attributed to the presence of Mn impurity.

Further lowering of the temperature leads to a next small maximum at 295 K, which is linked to the structural transition from the tetragonal to orthorhombic structure. This peak shows a complex structure consisting of two distinct humps, which are clearly separated. A next slight hump appears at 210 K for the heating run and at 187 K for the cooling one. The DSC experiments performed in the heating run exhibit that the Mn ion impurities influence the phase transition behaviour. The temperatures corresponding to the peaks and the enthalpy changes ΔH are collected in Table 1. The analysis of the experimental data presented in Table 1 testifies that the substitution of titanium for manganese in the amount of 0.1 wt. % causes large enthalpy changes, when compared with the pure BT. Qualitatively, the enthalpy changes can be used while describing ‘tetragonality’ of the BT ceramics (for the case of $x \geq 0,1$). Further studies in this direction are being planned.

Table 1. Characteristics of DSC peaks observed for BaTiO₃, BaTiO₃ + 0.01 wt. % MnO₂ and BaTiO₃ + 0.1 wt. % MnO₂ in the cooling run ($\beta = 10$ K/min). Enthalpy change ΔH is calculated from heat flow data, using a sigmoidal-type baseline. ΔH values are determined with the accuracy better than 1%.

Samples	Peak at T , [K]	ΔH [mJ/g]	Peak at T , [K]	ΔH [mJ/g]	Peak at T [K]	ΔH [mJ/g]
BaTiO ₃	392	1055	273	442	184	207
BaTiO ₃ + 0.01 wt. % MnO ₂	394	1095	278	493	188	260
BaTiO ₃ + 0.1 wt. % MnO ₂	393	882	278	320	187	50

3.3. Dielectric investigations

Dielectric properties of the ceramics BaTiO₃, BaTiO₃ + 0.01 wt. % MnO₂ and BaTiO₃ + 0.1 wt. % MnO₂ can be described by the temperature dependences of the real part ϵ' of the dielectric permittivity (see Fig. 4 and Fig. 5) and the electric conductivity σ' in the heating run. Fig. 4 shows the curves $\epsilon'(T)$ for the selected set of electric field frequencies. For all of the samples, the temperatures where three maxima ϵ' occur overlap for all the frequencies studied by us. In the case of ferroelectric ceramics, these maxima correspond to the structural phase transitions for both the BT and the Mn-doped samples, and a sharp paraelectric–ferroelectric (PE–FE) phase transition occurs at 403 K. This transformation is caused by the structural tetragonal–cubic change. Doping of the BT ceramics with a small amount of Mn ions (0.01 wt. %) results in increasing dispersion in the whole temperature region. At the same time, the maximum dielectric permittivity ϵ' at the PE–FE phase transition decreases by a half, when compared to that observed for the pure BaTiO₃.

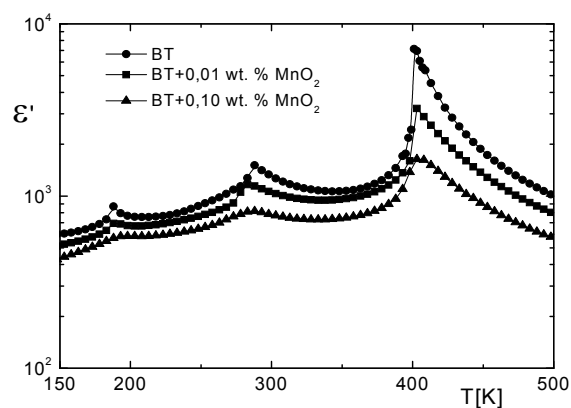


Fig. 4. Temperature dependences of real parts of the complex dielectric permittivity (ϵ') for BaTiO₃, BaTiO₃ + 0.01 wt. % MnO₂, and BaTiO₃ + 0.1 wt. % MnO₂ samples (a heating run).

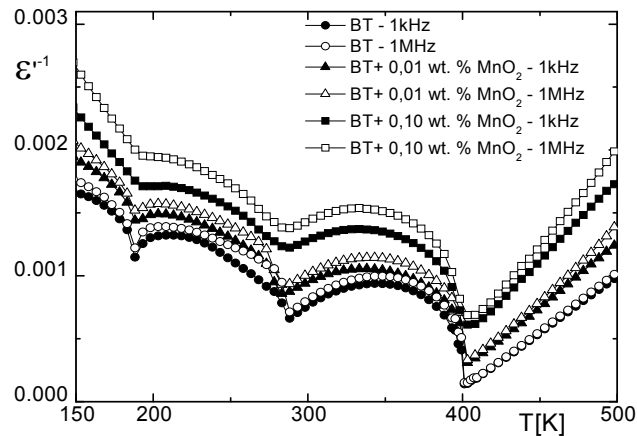


Fig. 5. Inverses of real parts of complex dielectric permittivity ($1/\epsilon'$) as functions of temperature for the samples of BaTiO₃, BaTiO₃ + 0.01 wt. % MnO₂ and BaTiO₃ + 0.1 wt. % MnO₂, as measured at different frequencies in the heating run.

The increase in Mn content up to 0.1 wt. % results in even greater dispersion and further reduction of the maximal dielectric permittivity. For the pure BaTiO₃ and BaTiO₃ + 0.01 wt. % MnO₂, the phase transition between the tetragonal and orthorhombic phases occurs at 288 K, while the same transition for BaTiO₃ + 0.1 wt. % MnO₂ is seen at 283 K. After the temperature is lowered by about 100 K, the next maxima appear on the curves $\epsilon'(T)$. They correspond to the orthorhombic–rhombohedral transformation. Increasing Mn content in the BT causes a gradual diffusion of all the phase transformations and, in particular, the PE–FE phase transition seen in the temperature dependence of the dielectric permittivity.

The constants C and T_0 for a number of frequencies, which have been obtained in the heating run from the linear regression, are presented in Table 2. The analysis of the data shown in Table 2 testifies that the greatest difference in the parameters is observed for the samples of BaTiO₃ + 0.1 wt. % MnO₂. For the samples doped with manganese, the Curie–Weiss constant is about 10^4 , which is characteristic for the order-disorder phase transitions.

Table 2. Dielectric parameters of BaTiO₃, BaTiO₃ + 0.01 wt. % MnO₂ and BaTiO₃ + 0.1 wt. % MnO₂, as measured in the heating run.

Samples	f [kHz]	C [K]	T_0 [K]
BaTiO ₃	1	$(1.12 \pm 0.004) \times 10^5$	388 ± 0.94
	10	$(1.08 \pm 0.006) \times 10^5$	389 ± 0.26
BaTiO ₃ + 0.01 wt. % MnO ₂	1	$(9.91 \pm 0.005) \times 10^4$	375 ± 0.23
	10	$(8.80 \pm 0.01) \times 10^4$	378 ± 0.56
BaTiO ₃ + 0.1 wt. % MnO ₂	1	$(7.90 \pm 0.004) \times 10^4$	361 ± 0.89
	10	$(6.75 \pm 0.004) \times 10^4$	366 ± 0.67

The a. c. conductivities obtained for our samples at 100 Hz are presented in Fig. 6. In the phase transition region of 420–450 K, the value of the a. c. conductivity reaches local maximums for the pure BT and each value of the Mn concentration. This has been explained earlier by Heywang [16, 17] who predicted such a behaviour basing on the acceptor state density at the grain boundaries, the charge carrier density and the energy gap between the conduction band and the

acceptor levels. A PTCR (Positive Temperature Coefficient Resistor) effect is observed in the phase transition region. The increase in the resistivity seen above the Curie temperature is caused by potential barriers located at the grain boundary and trapping of electric carriers through the polar regions. The straight-line segments in Fig. 6 seen in the high-temperature region indicate that the electric conductivity can be described by the relation

$$\sigma = \sigma_0 e^{-\frac{\varphi}{kT}}, \quad (1)$$

where k is the Boltzmann constant, σ_0 the pre-exponential factor, and φ the activation energy.

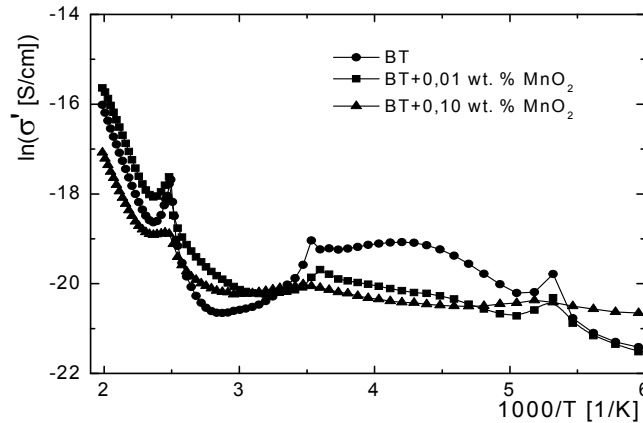


Fig. 6. Dependences of a. c. conductivity upon reciprocal temperature for the samples of BaTiO₃, BaTiO₃ + 0.01 wt. % MnO₂ and BaTiO₃ + 0.1 wt. % MnO₂ (a heating process).

Using this formula, we have calculated the activation energy of the electric conductivity for the temperature region above 430 K. The parameters obtained by us are $\varphi_1 = 0.68 \pm 0.006$ eV, $\varphi_2 = 0.64 \pm 0.005$ eV and $\varphi_3 = 0.55 \pm 0.009$ eV for the pure BaTiO₃, BaTiO₃ + 0.01 wt. % MnO₂ and BaTiO₃ + 0.1 wt. % MnO₂, respectively. Since the similar values are obtained for the activation energy, the same transport mechanism for the electric charges is expected to occur in all of the samples under investigation. However, the activation energies typical for semiconductors should depend on the free electric charge and the bound charge [16]. The value obtained here agrees with the activation energy derived for the electron case of hopping in the perovskite materials containing titanate.

In the Kroger–Vink notation, the properties of the undoped BaTiO₃ ceramics may be described by the following equation [18–22]:



where $\text{V}_\text{O}^{\bullet\bullet}$ denotes the oxygen vacancy with the effective charge of 2^+ . The produced electrons are almost fully delocalised by a hopping motion from one titanate site to another, according to the equation [18–22]



where $\text{Ti}_\text{Ti}^{\times}$ is the Ti ion (Ti^{4+}) sitting on the Ti lattice site with a neutral charge, and Ti_Ti' is the Ti

ion (Ti³⁺) sitting on the Ti lattice site with a single negative charge. When we incorporate the Mn dopants which can exist in the three valence states (Mn²⁺, Mn³⁺ and Mn⁴⁺), the electrons can also bond to the Mn ions in accordance with the schemes (see [18–26])



Here Mn_{Ti}[×] is the Mn ion sitting on the Ti lattice site with a neutral charge, Mn_{Ti}' is the Mn ion sitting on the Ti lattice site with a single negative charge, and Mn_{Ti}'' is the Mn ion sitting on the Ti lattice site with a double negative charge. Let us take into account that the Mn³⁺ ions in the Mn³⁺-doped BaTiO₃ crystals can occupy Ti⁴⁺ sites, due to close ionic radiuses [10]. The generated electrons are preferentially trapped by the Mn ions. Therefore the amount of manganese ions is very low due to very low Mn concentrations, and the motion of electrons from one Mn site to another can be effectively suppressed. This causes localisation of electrons on the Mn sites and, thus leading to changing potential barrier of the grain boundary. The mechanism presented here is believed to be responsible for the resistance behaviour of the variable-valence acceptors in the BaTiO₃ + *x* wt. % MnO₂ system.

4. Conclusions

The polycrystalline samples of BaTiO₃, BaTiO₃ + 0.01 wt. % MnO₂ and BaTiO₃ + 0.1 wt. % MnO₂ have been obtained by means of a conventional ceramic technology. The materials thus synthesised have been examined using the SEM. The EDS measurements have revealed that the samples are perfectly sintered and chemically homogeneous and confirmed a high quality of the latter. The DSC experiments performed in the heating run have testified the influence of Mn impurity on the behaviour of phase transitions. The values obtained for the enthalpy changes ΔH indicate that the substitution of titanium for manganese in the amount of 0.1 wt. % causes significant enthalpy changes, when compared with those occurring in the pure BT. The dielectric measurements have shown that the parameters of our samples are sensitive to the frequency of the applied electric field. The activation energy of the electric conductivity for the temperatures above 430 K has been calculated. The PTCR effect has been observed in the region of phase transition. Increasing content of Mn ions in the BT has been shown to cause gradual diffusion of all the phase transformations and, in particular, the PE–FE phase transition.

References

1. Kishi H, Mizuno Y and Chazono H, 2003. Base-metal electrode-multilayer ceramic capacitors: past, present and future perspectives. *Japan. J. Appl. Phys.* **42**: 1–15.
2. Randall C A, 2001. Scientific and engineering issues of the state-of-the-art and future multilayer capacitors. *J. Ceram. Soc. Japan.* **109**: S2–S6.
3. Tillmanns E, Hofmeister W and Baur W H, 1985. Variations on the theme of closest packing: the structural chemistry of barium titanate compounds. *J. Solid State Chem.* **58**: 14–28.
4. Kirby K W and Wechsler B A, 1991. Phase relations in the barium titanate–titanium oxide system. *J. Am. Ceram. Soc.* **74**: 1841–1947.
5. Jona F and Shirane G. *Ferroelectric crystals*. New York: Macmillan (1962).
6. Keith G M, Rampling M J, Sarma K, McAlford N and Sinclair D C, 2004. Synthesis and characterization of doped 6h-BaTiO₃ ceramics. *J. Eur. Ceram. Soc.* **24**: 1721–1724.
7. Kirianov A, Ozaki N, Ohsato H, Kohzul N and Kishi H, 2001. Studies on the solid solution of

- Mn in BaTiO₃. Japan. J. Appl. Phys. **40**: 5619–5623.
8. Wei X K, Zhang Q H, Li F Y, Jin C Q and Yu R C, 2010. Structural evolution induced by acceptor doping into BaTiO₃ ceramics. J. Alloys Compd. **508**: 486–493.
 9. Hennings D F K, 2001. Dielectric materials for sintering in reducing atmospheres. J. Eur. Ceram. Soc. **21**: 1637–1642.
 10. Tsur Y, Dunbar T D and Randall C A, 2001. Crystal and defect chemistry of rare earth cations in BaTiO₃. J. Electroceram. **7**: 25–34.
 11. Wang S F, Wang Y R, Wu Y C and Liu Y J, 2009. Densification, microstructural evolution and dielectric properties of hexagonal Ba(Ti_{1-x}Mn_xO₃) ceramics sintered with fluxes. J. Alloy. Compd. **480**: 499–504.
 12. Rödel J, Tomandl G, 1984. Degradation of Mn-doped BaTiO₃ under high d. c. electric field. J. Mat. Sci. **19**: 3515–3523.
 13. Garbarz - Glos B, Bormanis K and Sitko D, 2011. Effect of Zr⁴⁺ doping on the electrical properties of BaTiO₃ ceramics. Ferroelectrics **417**: 118–123.
 14. Shvartsman V V, Kleemann W, Dec J, Xu Z K and Lu S G, 2006. Diffuse phase transition in BaTi_{1-x}Sn_xO₃ ceramics: an intermediate state between ferroelectric and relaxor behaviour. J. Appl. Phys. **99**: 124111–124119.
 15. Capsal J F, and Pousserot Ch, Dantras E, Dandurand J and Lacabanne C, 2010. Dynamic mechanical behaviour of polyamide 11/Barium titanate ferroelectric composites. Polymer. **51**: 5207–5211.
 16. Heywang W, 1961. Barium titanate as a semiconductor with blocking layers. Solid State Electron. **3**: 51–58.
 17. Heywang W, 1964. Resistivity anomaly in doped barium titanate. J. Am. Ceram. Soc. **47**: 484–490.
 18. Kröger F A and Vink H J. Solid state physics, Vol. 3. New York: Academic Press (1956).
 19. Smyth D M. The defect chemistry of metal oxides. New York: Oxford University Press (2000).
 20. Hagemann H J and Hennings D F K, 1981. Reversible weight change of acceptor doped barium titanate. J. Am. Ceram. Soc. **64**: 590–594.
 21. Lee D K, Yoo H I and Becker K D, 2002. Nonstoichiometry and defect structure of Mn-doped BaTiO_{3-δ}. Solid State Ionics. **154–155**: 189–193.
 22. Aksel E, Jakes P, Erdem E, Smyth DM, Ozarowski A, van Tol J, Jones J L and Eichel R A, 2011. Processing of manganese-doped [Bi_{0.5}Na_{0.5}]TiO₃ ferroelectrics: reduction and oxidation reaction during calcinations and sintering. J. Am. Ceram. Soc. **94**: 1363–1367.
 23. Takezawa Y, Kobayashi K, Nakasone F, Suzuki T, Mizuno Y and Imai H, 2009. Mn-doped BaTiO₃ thin film sintered using nanocrystals and its dielectric properties. Japan. J. Appl. Phys. **48**: 111408–111413.
 24. Eichel R A, 2007. Defect structure of oxide ferroelectrics—valence state, site of incorporation, mechanisms of charge compensation and internal bias fields. J. Electroceram. **19**: 9–21.
 25. Erdem E, Jakes P and Eichel R A, 2010. Formation of (TiTi–V••O)• defect dipoles in BaTiO₃ ceramics heat-treated under reduced oxygen partial-pressure. Functional Mater. Lett. **3**: 65–68.
 26. Eichel R A, 2011. Structural and dynamic properties of oxygen vacancies in perovskite oxides—analysis of defect chemistry by modern multi-frequency and pulsed EPR techniques. Chem. Phys. **13**: 368–384.

Sitko D., Bał W., Garbarz-Głós B., Antonova M. and Jankowska-Sumara I., 2012.
Effect of MnO₂ doping on the dielectric properties of barium titanate ceramics.
Ukr.J.Phys.Opt. **13**, Suppl. 3: S34 – S43.

***Анотація.** У роботі досліджено вплив легування MnO₂ на структуру, мікроструктуру і діелектричні властивості BaTiO₃. Для цього було підготовлено кераміку BaTiO₃, леговану MnO₂, згідно із загальноприйнятим методом. За методом енергодисперсійної X-спектроскопії виявлено різне спікання зразків зі складом BaTiO₃+ x ваг. % MnO₂ (x = 0,01; 0,1). Встановлено, що електричні параметри кераміки залежать від частоти електричного поля і концентрації заміщення. Для кращого розуміння характеру фазового переходу в системах BaTiO₃+ x ваг. % MnO₂ (x = 0,01; 0,1) було досліджено температурну поведінку діелектричних характеристик.*